K. Vini and K. M. Nissamudeen*

Facile Combustion Synthesis of $(Y,Pr)_2O_3$ Red Phosphor: Study of Luminescence Dependence on Dopant Concentration and Enhancement by the Effect of Co-dopant

https://doi.org/10.1515/zna-2019-0346 Received November 23, 2019; accepted January 28, 2020; previously published online March 7, 2020

Abstract: There occurs a great interest in explaining the dependence of dopant concentration on the luminescence efficiency of rare earth oxides. Unambiguously, this study explains that luminescence intensity increases with increase in dopant concentration only up to optimised value. The syntheses of doped and co-doped yttrium oxide (Y₂O₃) nanophosphors in this study were carried out by making use of combustion method. This method produces the nanophosphors that have sizes ranging between 5 and 20 nm as confirmed by transmission electron microscopy. X-ray diffraction pattern confirms that the incorporation of praseodymium oxide (Pr^{3+}) and gadolinium oxide (Gd^{3+}) does not cause any change in the cubic structure of Y₂O₃. The phase purity has been confirmed by Fourier transform infrared spectrum. Diffuse reflectance spectra reveal that the bandgap increases with increase in annealing temperature. Bandgap has been calculated by making use of the Kubelka-Munk function. Strongest emission was observed at 605 nm with 2 wt% of Pr3+ as optimised concentration. Replacement of Y³⁺ by Gd³⁺ partially enhances the 605-nm emission linearly. The [Y:Pr:Gd] exhibits luminescence intensity of 2.705 times more than that of Y:Pr nanophosphors. This is for the first time our team has made a detailed study regarding the effects of co-doping in the case of Y₂O₃:Pr powders. We have successfully presented the changes that happen to the particle after co-doping especially in the particle size and luminescence properties.

Keywords: Doping; Energy Transfer; Luminescence; Phosphors; Y_2O_3 Particles.

K. Vini: School of Pure and Applied Physics, Kannur University, Payyanur, India, E-mail: viniravindran24@gmail.com

1 Introduction

Phosphors play an important role in display applications. Some of the significant features of this type of applications are long life and high luminescence properties. Researches have been done extensively to find the ways to increase the luminescence of nanophosphors. One such method is the incorporation of rare earth elements as dopants into the host lattice [1]. White light-emitting diodes (LEDs) are under extensive study and have become a hot topic in terms of both their fundamental and technological importance because of their reduced volume, long life span, high efficiency, free of mercury pollution, and conservation of energy [2-6]. Fabrication of white LEDs can be done by many ways. It can be done either by the combination of single near-ultraviolet (UV) LED with red-blue-green (RGB) colour phosphor or by the combination of blue LED with vellow phosphor. In the last decade, detailed investigation has been carried out by the researchers on the red light-emitting phosphors by doping with europium oxide $(Eu^{2+} \text{ and } Eu^{3+})$ [7]. Yttrium oxide (Y_2O_3) doped with Eu^{3+} nanophosphors exhibits high-luminescence phenomena under cathode ray and UV excitation [8]. Later, many scientists reported the red light-emitting properties of samarium oxide (Sm $^{3+}$) when it incorporates into Y₂O₃ under the excitation [7]. This work mainly focussed on luminescence properties of praseodymium (Pr)-doped Y2O3 nanophosphors. Although some work has been done in connection with Pr-doped nanophosphors, still much more work has to be done on this topic to get deep inside into Physics [9]. Praseodymium oxide is one among the rare earth elements that can be used as red light-emitting phosphors in the host lattice [10]. Light-emitting properties of Pr³⁺ depend on the nature of the host lattice. The lanthanum oxide (La₂O₃) doped with Pr³⁺ emits green colour, but in the case of cubic Y_2O_3 doped with Pr^{3+} , emission of red light prevails. The up-conversion properties of Y₂O₃ doped with Pr³⁺ have been paid much more attention because of its application in short-wavelength laser [11].

Traditionally, synthesis of phosphors has been done by solid-state reactions. The particle size, synthesised by this method, is in micrometer range. The process of grinding is required to convert larger phosphors into smaller one. Unfortunately, some additional defects are reported

^{*}Corresponding author: K. M. Nissamudeen, School of Pure and Applied Physics, Kannur University, Payyanur, India, E-mail: nisamkm@gmail.com

because of this grinding process, which in turn reduces the luminescence properties. However, combustion method results in the preparation of small sized phosphors at low temperature with less time [7]. This article reports the preparation of Y_2O_3 : Pr^{3+} red phosphor by combustion reaction and luminescence enhancement by the addition of co-dopant.

2 Experimental

For synthesis work, Y₂O₃, praseodymium oxide (Pr₂O₃), nitric acid (HNO₃), and citric acid (C₆H₈O₇) were used as the precursor materials. The chemicals that we take are of analytical grade, purchased from Sigma-Aldrich (99.99 %, Bengaluru) and used without further purification. 0.99 g of Y2O3 and 0.01 g of Pr2O3 (total of 1 g) were dissolved in a mixture of solution containing 25 mL of deionised water and 25 mL of concentrated HNO3. We know that most of the rare earth oxides are insoluble in water. Thus, we added HNO3 as one of the solvents and then heat at 373 K for 2 h with constant stirring. When the solution started boiling, first fumes appeared, and then the solution turned milky white colour. Finally, solution resulted into a transparent solution and was viscous in nature. The metallic ions required for the reaction were present in the solution. When the solution cooled, we added $C_6H_8O_7$ [12]. The purpose of addition of $C_6H_8O_7$ is that it acts as a chelating agent in converting the solution to gel [13]. The amount of $C_6H_8O_7$ to metal solution is in the ratio 2:1 [12]. The metal-citrate complex was formed by the addition of C₆H₈O₇ to the metal solution, which suddenly precipitated out from the solution [12]. When the solution was heated at 373 K, the amount of solution slowly decreased, and the colour of the solution became pale yellow, which was due to decomposition of nitrate, and finally transparent sol was obtained. Further heating resulted to dehydration and hence caused the condensation reaction between acid groups with the formation of water. Removal of excess water resulted in the transformation of sol into transparent gel [13]. The remaining gel has been collected in silica/alumina crucible and annealed to 773 K for 3 h in the furnace with the heating rate of 333 K/h. Finally, we obtained sandal colour Y₂O₃:Pr nanopowders. We repeated the experiment by changing the concentration of Pr and obtained the optimised concentration followed by annealing at various temperatures. With the optimised concentration, we extended our study on the effect of pH, which is one of the important parameters for size tailoring and Pr³⁺ luminescence. By the addition of ammonium hydroxide, the pH of the solution varied from 4 to 10, and the dependence of luminescence on pH was studied. In the second step, Y₂O₃:Pr has been co-doped with Gd³⁺, and the detailed study regarding the aftereffects of co-doping was performed.

The structure and crystallinity of the powders were analysed by X-ray diffraction (XRD) using Rigaku Miniflex 600, Mumbai ($\lambda=0.15406$ nm, 40 kV, 15 mA). The phase purity of the samples was studied using Fourier transform infrared spectrum (FTIR) in the wavelength range of 400–4000 cm $^{-1}$ using Cary 630 with ATR (Agilent Technologies, Bengaluru). Diffuse reflectance spectra (DRSs) of samples prepared by the present method were analysed using UV-Vis spectrophotometer (Lambda; PerkinElmer, Thane) in the wavelength range of 200–800 nm. The studies regarding photoluminescence (PL) were characterised on Cary Eclipse Fluorescence Spectrometer

(Agilent Technologies, Bengaluru). The studies related to the size and morphology of powders were carried out by JEM-2100 (Jeol, Tokyo, Japan) high-resolution transmission electron microscopy (TEM). The machine was operating at an accelerating voltage of 200 kV.

3 Results and Discussion

3.1 Structural Analysis

3.1.1 X-ray Diffraction

At present, we have focussed on the optimisation of the optical properties of the powder as a function of Pr concentration. 2 wt% of Pr³⁺-doped Y₂O₃ powder seems to be the maximum in the case of luminescence intensity when compared with other Pr³⁺ concentrations [14]. Figure 1a shows the XRD studies of the phase formation of pure Y₂O₃ and 2 wt% Pr³⁺-doped Y₂O₃ powders. The XRD pattern confirms that the product formed is of single-phase compound. This was revealed from the nature of the diffraction peaks, which were single and sharp [15]. The pure Y_2O_3 nanoparticles and 1173 K-annealed Pr^{3+} -doped Y_2O_3 powders exhibit identical XRD pattern [16]. The ionic radius of Pr^{3+} is 1.13 A^0 , and that of Y^{3+} is 0.90 A^0 , which are very close. Thus, the substitution of Y³⁺ with Pr³⁺ ions is easily possible. The results give evidence that the crystal structure remains the same even after the incorporation of Pr^{3+} into the host Y_2O_3 lattice [15]. Quite interestingly, it has been noted that all the peaks including minor peaks correspond to Y₂O₃, which indicates that the Pr₂O₃ is properly substituted into Y_2O_3 , although the ionic radius of Y^{3+} is slightly smaller than Pr^{3+} ions [17]. This, in turn, confirms that the method that we adopted is excellent for doping by making powders with the substitution of Pr in the host Y_2O_3 [17]. The (hkl) values of all the peaks are indexed in the XRD studies. The diffraction peaks are indexed in accordance with the JCPDS file no. 41-1105. It confirms that the obtained samples have cubic structure [7, 18]. The unit cell lattice parameters were $a = b = c = 10.60 \text{ A}^0$ with $\alpha = \beta = \gamma = 90^{\circ}$ [15]. The strongest peak appeared to be at $2\theta = 29.15$. This corresponds to (222) plane for all the compounds. No other extra peaks were noticed, which indicates the presence of impurities [15].

The XRD studies of 2 wt% Pr^{3+} -doped Y_2O_3 phosphors in synthesised temperature and annealed at different temperatures are shown in Figure 1b. During the phase evaluation, the obtained diffraction peaks reveal that the incidence of X-rays on the as-prepared sample shows amorphous nature [19]. At this stage, there appear wide diffraction peaks. The wider peaks can be correlated

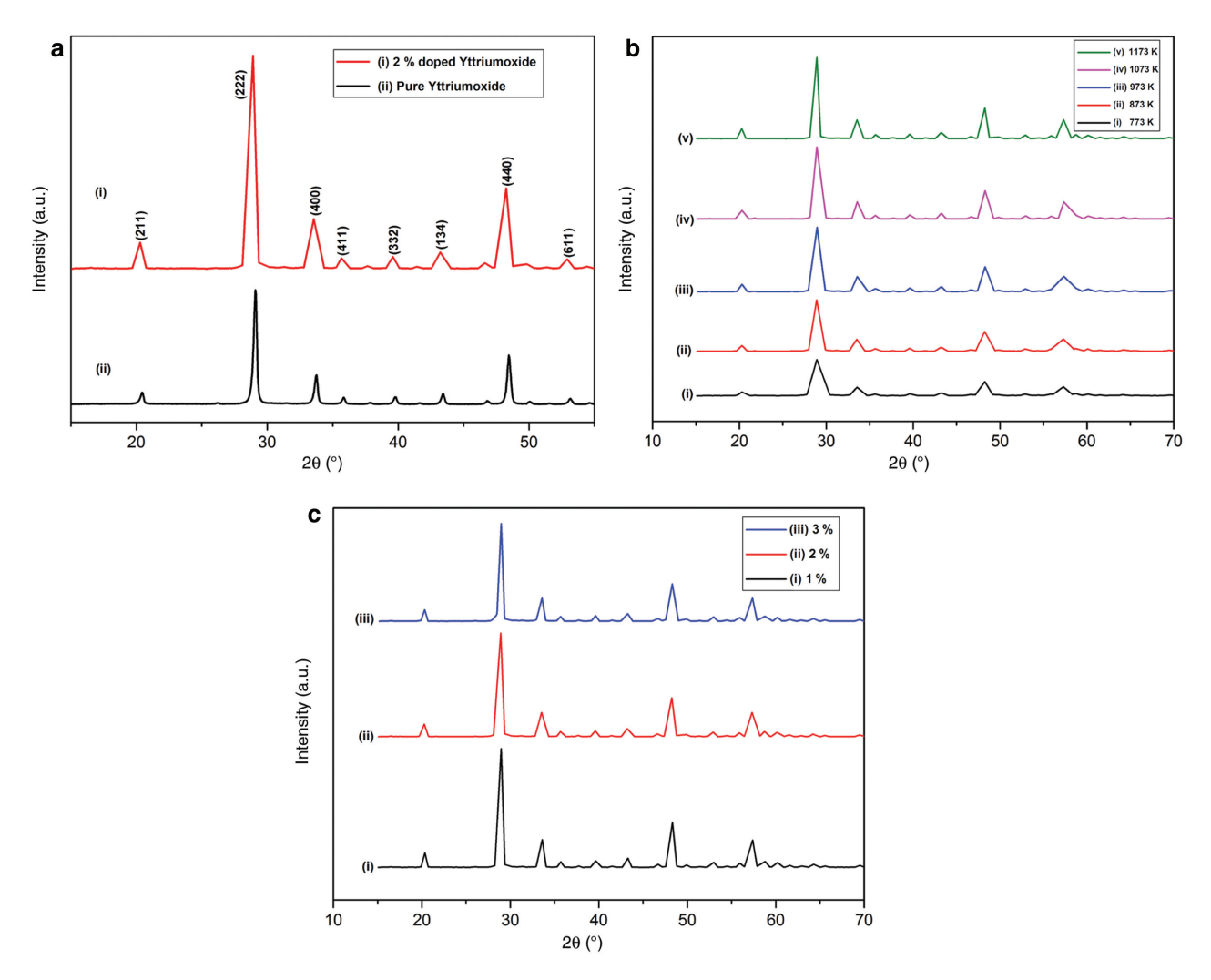


Figure 1: XRD spectra of (a) undoped and 2 wt% Pr^{3+} -doped samples, (b) 2 wt% Pr^{3+} -doped samples annealed at different temperatures, and (c) samples of various Pr^{3+} concentrations annealed at 1173 K.

to the smaller crystallite size [17]. Further, the process of annealing results in the phase transformation of the samples from amorphous to crystalline of Pr3+-doped Y2O3 nanoparticles [17]. The crystallinity improvement with annealing temperature may be because of the enhanced oxidation kinetics [20]. The final product that we synthesised by the combustion method is of highly crystalline nature. This was confirmed by the presence of strong and sharp diffraction peaks that the sample exhibits [21]. This strongly reveals the dependence of the crystallite size and crystallinity of the Pr-doped Y₂O₃ nanoparticles on the annealing temperature [17]. As far as the phosphors are considered, this is very important because high crystallinity usually means less defects and bright luminescence [21]. The FWHM value of the peak is high for assynthesised samples when compared to samples annealed at higher temperature. It was expected that when the annealing temperature of the samples increases, the width

of the peak becomes narrower. Clearly, this is because of the enhancement in crystallinity of the Pr³⁺-doped Y₂O₃ nanopowders [22]. There occurs size increment from 7 to 17 nm when the samples annealed from 773 to 1173 K, respectively [23]. Crystallite size grows with temperature. In the case of nanophosphors, when the size of the grain increases, surface area of the particles decreases, which in turn increases the luminescence intensity. This can be due to the reduction of surface defects as well as the nonradiative rates [14]. When the annealing temperature increases, the lattice parameter decreases, and the crystallite size increases. This indicates that the lattice plane was so close, which in turn led to enhancement of density and reduction of dislocation density [24]. Moreover, there appears the presence of tensile strain and reduction of lattice constant. This was confirmed through the shifting of peaks towards longer angles as the temperature increases [24].

Determination of crystallite size can be done from the most intense peak by making use of Scherrer equation. Calculation of lattice parameter and lattice constant was also done.

One interesting and important observation is that the particle size increases with increase in dopant concentration annealed at a particular temperature, as shown in Figure 1c [22]. But the quenching process of luminescence occurs when the dopant concentration exceeds a particular value, and this will be discussed in detail later [21]. Praseodymium atom is heavier than yttrium, so this difference in their mass may play an important role during synthesis reaction of growth process through diffusion [22]. A slight increase was observed in the lattice parameter when the Pr³⁺ concentration increases. This is clear because Pr³⁺ has a larger ionic radius when compared to Y³⁺. This systematic increase of lattice parameter confirms that the Pr³⁺ ions are properly incorporated into the host lattice [16]. This can be also confirmed from the diffraction peaks. The peaks are shifted towards smaller angles when

 Pr^{3+} concentration increases, which in turn confirms that Pr^{3+} is inserted properly into Y_2O_3 site [25].

Crystallite size is not the only factor that is responsible for the broadening of the peak. Presence of strain also plays an important role [15]. The effects of both in the case of peak broadening are not dependent on each other. They can be studied by the Hall–Williamson plot. Figure 2a shows the Hall–Williamson plot to calculate the strain. The strain value (ε) that we obtained is found to be minute, which is of the range 10^{-3} , which indicates its effect is negligible [15].

Calculations of particle density, dislocation density, FWHM, lattice parameter, strain, and crystallite size are tabulated in Table 1. The Rietveld refinement was employed purely to confirm the cubic structure of the assynthesised sample. The data points were refined using the FULLPROF program. Figure 2b represents the Rietveld refinement of the calcined Y_2O_3 :2 wt% Pr:1 wt% Gd sample. The experimental and stimulated XRD intensities are in agreement with each other [26, 27].

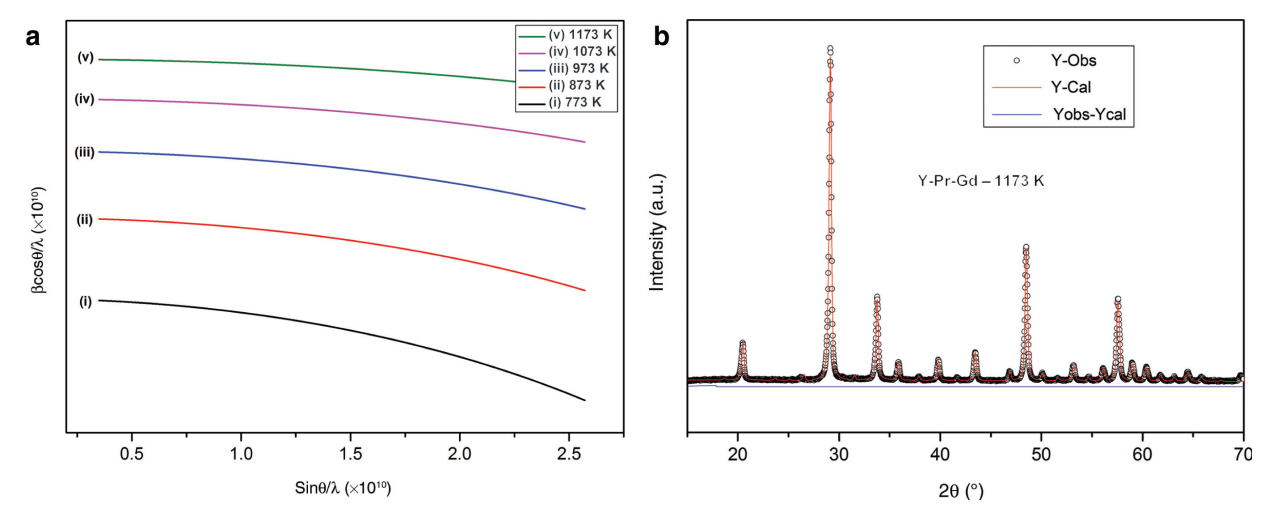


Figure 2: (a) Hall Williamson plot to calculate the strain. (b) Rietveld refinement of Y₂O₃:2 wt% Pr:1 wt% Gd phosphor.

Table 1: Structural parameters of doped Y₂O₃ phosphors.

Temperature (K) of 6 wt% Eu ³⁺	FWHM (β) (degree)	Lattice parameter a (Aº)	Crystallite size D (nm) Debye-Scherrer	Interplanar spacing	Dislocation density (δ)	Particle density (Dx) g/cm ³	Microstrain (ε) (10 ⁻³)
873	0.82835	10.6373	9.90	3.0707	1.02	4.9844	-0.0173
973	0.7707	10.6355	10.64	3.0702	0.88	4.9869	-0.0161
1073	0.69987	10.6250	11.71	3.0671	0.72	5.0017	-0.0146
1173	0.48747	10.6158	16.81	3.0645	0.35	5.0148	-0.0102
Concentration (%)	of samples ar	nnealed at 1173 K					
1 %	0.53608	10.6094	15.29	3.0626	0.42	5.0238	-0.0112
2 %	0.48747	10.6158	16.81	3.0645	0.35	5.0148	-0.0102
3 %	0.49479	10.6308	16.57	3.0688	0.36	4.9936	-0.0103

Optimised dopant concentration is obtained when we add 2 wt% of Pr3+ to Y2O3. To this optimised dopant concentration, we add different percentages of Gd₂O₃ as co-dopant. After co-doping with Gd³⁺, optimised concentration is obtained when Pr^{3+} is at 2 wt% and Gd^{3+} is at 1 wt%. The addition of dopant and co-dopant does not cause any change in the structure of the host. Figure 3a shows the XRD spectra of co-doped samples (Gd³⁺ 1 wt%) annealed at different temperature, and Figure 3b shows the XRD spectra of various co-dopant concentrations annealed at 1173 K [28]. After co-doping with Gd³⁺, all the peaks including minor peaks correspond to Y₂O₃ structure with Ia3 as space group. This was confirmed from the JCPDS file no. 43-1036. Shifting of peak appears when the temperature increases. The most intense peak that corresponds to (222) plane was found to be at $2\theta = 29.154$, 29.153, 29.153, 29.15, and 29.15 annealed at 773, 873, 973, 1073, and 1173 K, respectively. This confirms the formation of homogeneous powder at higher annealing temperature by redistribution of Y^{3+} , Pr^{3+} , and Gd^{3+} that possess different sizes via interdiffusion. The concentration gradients present in the precursor are responsible for the redistribution of cations [29]. Addition of co-dopant results in an increment of lattice parameter. This also confirms that the obtained oxides are homogeneous in nature [29]. Addition of co-dopant does not cause any change in the phase and crystal structure. But crystallite size increases. Moreover, lattice energy change exhibits lattice strain [17]. Obviously, it has been found that incorporation of Gd into Y_2O_3 site acts as self-promoter to attain good crystallisation [30]. Table 2 summarises the calculated values.

3.1.2 Fourier Transform Infrared Analysis

The FTIRs of undoped, Pr³⁺-doped, and Gd³⁺ co-doped yttrium nanophosphors in the range 400–4000 cm⁻¹ are shown in Figure 4a and b [18]. This FTIR spectrum

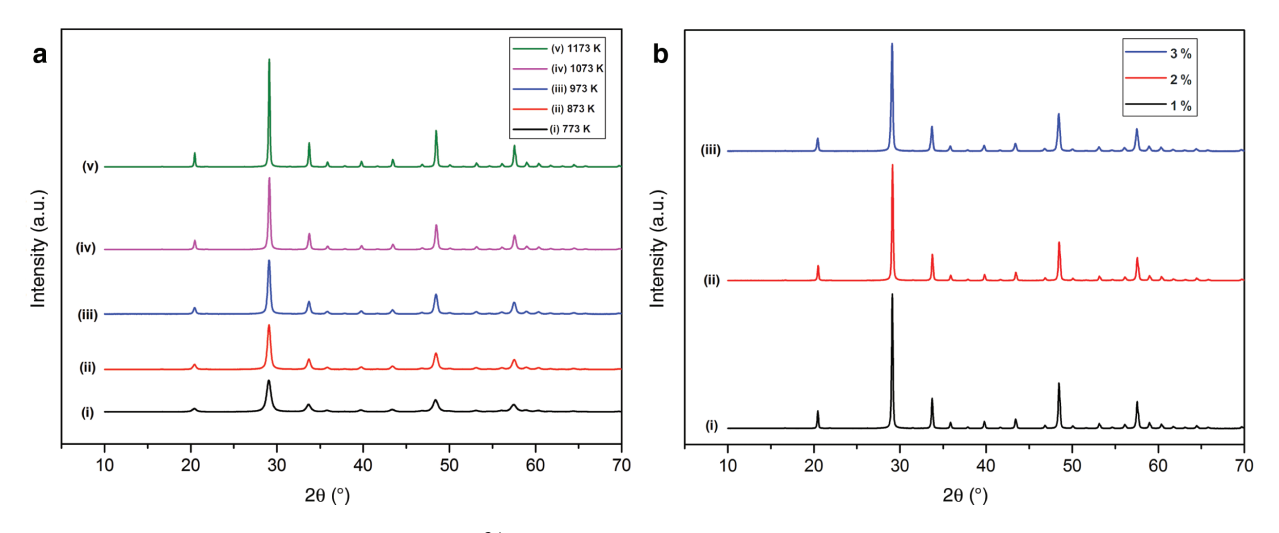


Figure 3: XRD spectra of co-doped samples. (a) Gd^{3+1} wt% at different annealing temperatures and (b) various concentrations annealed at 1173 K.

Table 2: Structural parameters of co-doped Y₂O₃ phosphors.

Temperature (K) of 6 wt% Eu ³⁺ and	FWHM (β) (degree)	Lattice parameter a (A ⁰)	Crystallite size D (nm) Debye-Scherrer	Interplanar spacing	Dislocation density (δ)	Particle density (Dx) g/cm ³	Microstrain (ε) (10 ⁻³)
Gd ³⁺ 7 wt%							
773	0.66295	10.6427	12.37	3.0722	4.03	4.9768	-0.119
873	0.47461	10.6355	17.28	3.0702	4.02	4.9869	-0.08522
973	0.37781	10.6284	21.71	3.0681	4.00	4.9969	-0.06784
1073	0.28172	10.6212	29.12	3.0660	3.98	5.0071	-0.05058
1173	0.19902	10.6070	41.22	3.0619	3.95	5.0272	-0.03573
Concentration (%) of	samples ann	ealed at 1173 K					
1 %	0.19902	10.6070	41.22	3.0619	3.95	5.0272	-0.03573
2 %	0.19935	10.6141	41.15	3.0640	3.97	5.0172	-0.03579
3 %	0.25166	10.6355	32.59	3.0702	4.02	4.9869	-0.04519

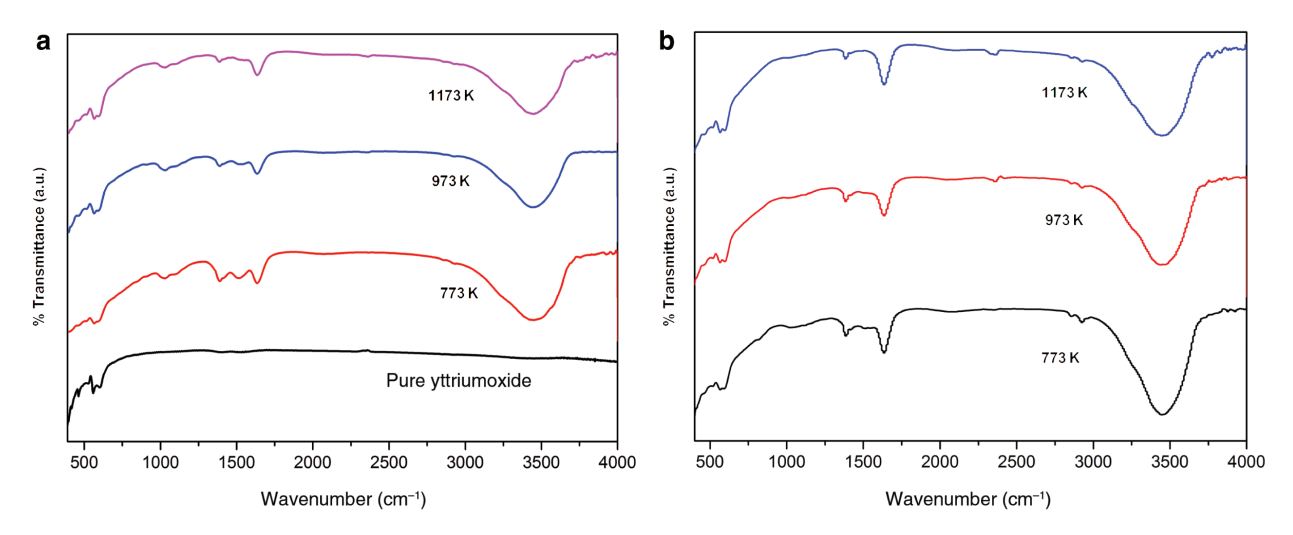


Figure 4: FTIR spectra of the prepared samples for different annealing temperatures (a) 2 wt% Pr^{3+} -doped Y_2O_3 , (b) 2 wt% Pr^{3+} and 1 wt% Gd^{3+} -co-doped Y_2O_3 .

indicates a band at 3452 cm⁻¹. The presence of OH⁻ stretching vibrations of hydrogen-bonded hydroxyl group is responsible for this band [31, 32]. This band is found to be weak in the case of pure yttrium compound [15]. This -OH group induces the luminescence quenching, which in turn results in the reduction of luminescence efficiency [15]. Elimination of this problem can be done by incorporating the step of annealing process [17]. From the FTIR spectra, it has been found that when the annealing temperature increases, the presence of this hydroxyl group (-OH) decreases [15]. The low band at 1637 cm⁻¹ was attributed to the presence of carbonate groups. This was formed due to CO2 molecules onto the surface of yttrium oxide [33, 34]. The C-O vibration bands are weak in the case of a pure Y_2O_3 nanophosphor. When the annealing temperature increases, vibration of C-O bond decreases. This confirms that the carbon content present in the sample decreases [15]. The band at 1385 $\,\mathrm{cm}^{-1}$ can be attributed to N-O stretching of NO₃⁻ group [35]. Here, annealing process also results in the reduction of NO₃⁻ residuals. The absorption peaks at 600 and 563 cm⁻¹ can be assigned to stretching vibrations of Y-O bond in Y₂O₃ lattice. This band favours the formation of cubic phase yttria in the case of Pr^{3+} -doped and Gd^{3+} -co-doped Y_2O_3 samples [35]. Here, annealing also plays a significant role. Excellent change occurs when the sample is annealed further [36]. When the annealing temperature reaches 1173 K, the organic residues almost vanish. Meanwhile, Y-O stretching bond becomes much stronger, which in turn confirms the perfect crystallisation of Y₂O₃ phosphor [36]. All the above discussed peaks together ensure that the Y_2O_3 nanophosphor has been formed [31]. The FTIR spectra show that the prepared samples do not contain

any organic residues that may result in the quenching of emission, as the same was confirmed by XRD studies [23, 32].

3.2 Optical Properties

3.2.1 Diffuse Reflectance Spectra

To characterise thin films, the UV-Vis absorption spectroscopy is usually used. In the case of films, scattering of light is very low. Thus, bandgap (Eg) values can be obtained easily if we know the thickness. However, in colloidal samples, the scattering effect is enhanced since a more superficial area is exposed to the light beam. In the case of normal incidence mode, dispersed light is considered as the same as that of absorbed light, and spectrum will not distinguish the two phenomena. Moreover, powdered samples can be obtained frequently instead of colloids or thin films. In UV-Vis absorption technique, sample is dispersed in fluid media such as methanol, ethanol, or water. If the sample size is large, it will precipitate and will be very difficult for the absorption of spectrum to interpret. To avoid these difficulties, it is better to use DRS, which supports the calculation of Eg of unsupported materials [15].

The DRSs of doped and co-doped Y_2O_3 nanophosphor annealed at different temperatures are shown in Figure 5 [37]. Here, CdSO₄ is taken as reference sample [15]. A band at 210 nm was obtained in the case of pure yttrium compound. This implies the absorption of this wavelength. Bandgap of the phosphor is responsible for this band [15]. For Pr^{3+} -doped Y_2O_3 samples, broad absorption band shows minimum absorption at 212

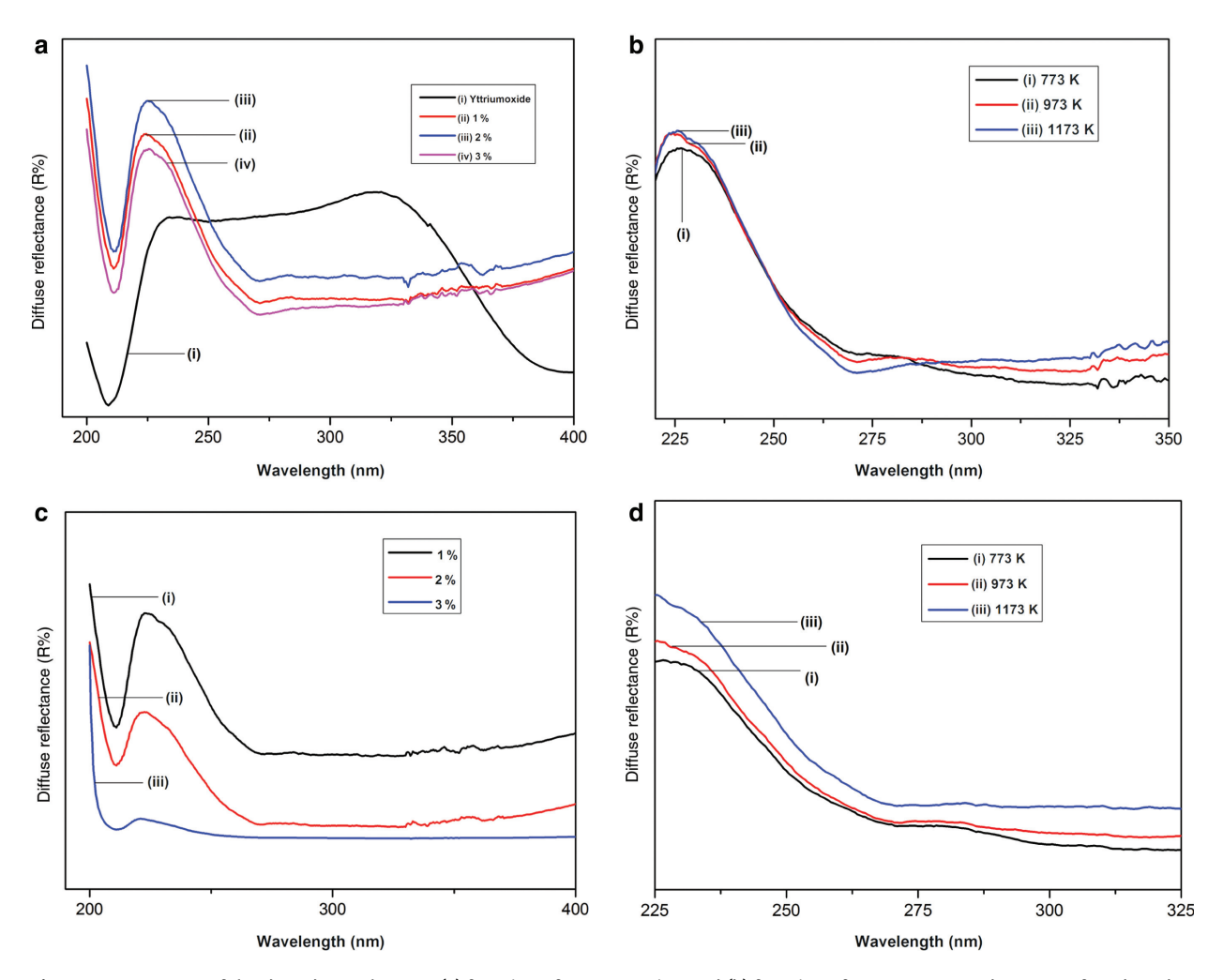


Figure 5: DR spectra of the doped samples as a (a) function of concentration and (b) function of temperature and spectra of co-doped samples as a (c) function of concentration and (d) function of temperature.

and 211 nm for Gd^{3+} co-doped samples [18]. This can be assigned to the transition between conduction and valence band [37]. The metastable energy level that occurs between conduction and valence band, by the addition of dopants, is responsible for the presence of other bands [15]. Absorption in UV-Vis region can be due to transactions concerned with defects or surface impurities. It is quite natural that small particles exhibit a large surfaceto-volume ratio, which in turn results in more defects. Thus, the small particles exhibit absorption band, which is broad and strong [37]. When we compare the absorption peak of as-prepared samples and annealed samples, a blue shift can be observed for as-prepared samples. This can be due to the smaller particle size of as-prepared samples when compared to annealed samples [17].

Bandgap determination is very important in solidstate physics [15]. The graph of $[F(R_8)hv]^2$ versus hv for pure, doped, and co-doped Y₂O₃ samples are shown in Figure 6 [17]. The energy difference between the top of the valence band, which is full of electrons, and bottom of the conduction band, which is free of electrons, is known as bandgap. Bandgap of semiconductors determines their application in the field of optoelectronics. Bandgap can be determined by making use of a method called Tauc-Plot. Using DRSs, bandgaps can be calculated by the Kubelka-Munk theory, which was proposed by two scientists named Kubelka and Munk [15].

By making use of the Kubelka-Munk function, the $[h\nu F(R_8)]^2$ was plotted along y axis and $h\nu$ along x axis. On the obtained curve, a line is drawn tangent to the point of inflection. The value obtained at the point of intersection of the tangent line along x axis is E_g (bandgap) [15]. The curve that we obtained exhibits both the linear and nonlinear portions. The linear part corresponds to the fundamental absorption, and the nonlinear part characterises absorption that contains impurity states [15]. The results that we obtained are in accordance with previous reports. This confirms the incorporation of Pr³⁺ into

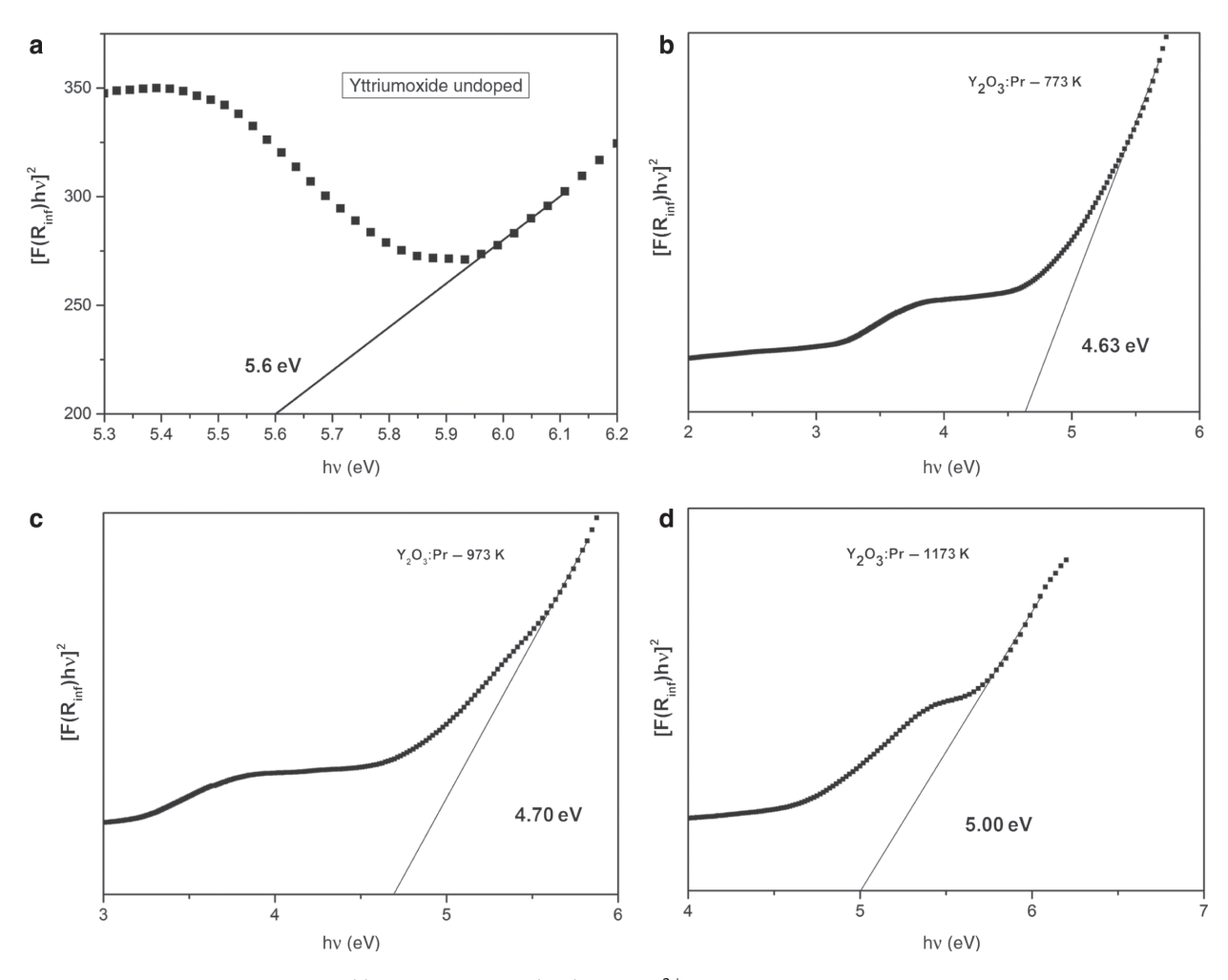


Figure 6: Bandgap calculation of the (a) undoped yttrium, (b-d) 2 wt% Pr^{3+} -doped samples annealed at different temperature and (e-g) 2 wt% Pr^{3+} 1 wt% Pr^{3+} 2 wt% Pr^{3+} 1 wt% Pr^{3+} 2 wt% Pr^{3+} 3 wt% Pr^{3+} 2 wt% Pr^{3+} 3 wt% Pr^{3+} 2 wt% Pr^{3+} 3 wt% Pr^{3+} 3 wt% Pr^{3+} 3 wt% Pr^{3+} 4 w

Y₂O₃ [17]. For doped samples, E_g values vary from 4.63 to 5.00 eV, and for co-doped samples, they vary from 3.99 to 4.42 eV. This bandgap difference can be because of size difference [15]. From the figure, it is clear that the E_g value is greater for annealed samples [37]. The lattice has certain degrees of structural order-disorder. This has influenced directly the distribution of intermediate energy level within the bandgap. There occurs the presence of structural defects in the case of as-prepared samples. Upon heat treatment, defects become less, and host matrix becomes ordered pattern. As a result, the minimisation of intermediate energy levels occurs within the bandgap, and finally E_g increases [37]. After co-doping with Gd^{3+} , the E_g value again reduces. This is because of the presence of oxygen vacancies created due to co-doping of Gd³⁺ ions. It is clear that Gd^{3+} is entrenched in Y_2O_3 lattice and produced oxygen vacancies, which in turn reduce the bandgap of nanophosphors [18]. The decrease in bandgap after co-doping is due to the increase in crystallite

size and crystal defects for the co-doped samples [38, 39].

3.2.2 Transmission Electron Microscopy

Transmission electron microscopy has been carried out to study the detailed structure of the particles and is shown in Figure 7. In order to obtain a good TEM image, the Pr-doped Y_2O_3 powder sample was dispersed in ethanol for around half an hour. Then, a drop is placed on the carbon-coated grid surface [12]. Field emission TEM (FE-TEM) image confirms that the obtained samples seem to be agglomerates that contain several crystallites with spherical shape [22]. This characterisation confirms the perfect crystalline nature of the nanophosphors. The obtained lattice fringe is found to be 0.306 nm. This is found to be in accordance with interplanar distance of (222) plane of Y_2O_3 nanophosphor [40]. The lattice fringes confirm that the nanophosphors that we obtained are of high quality.

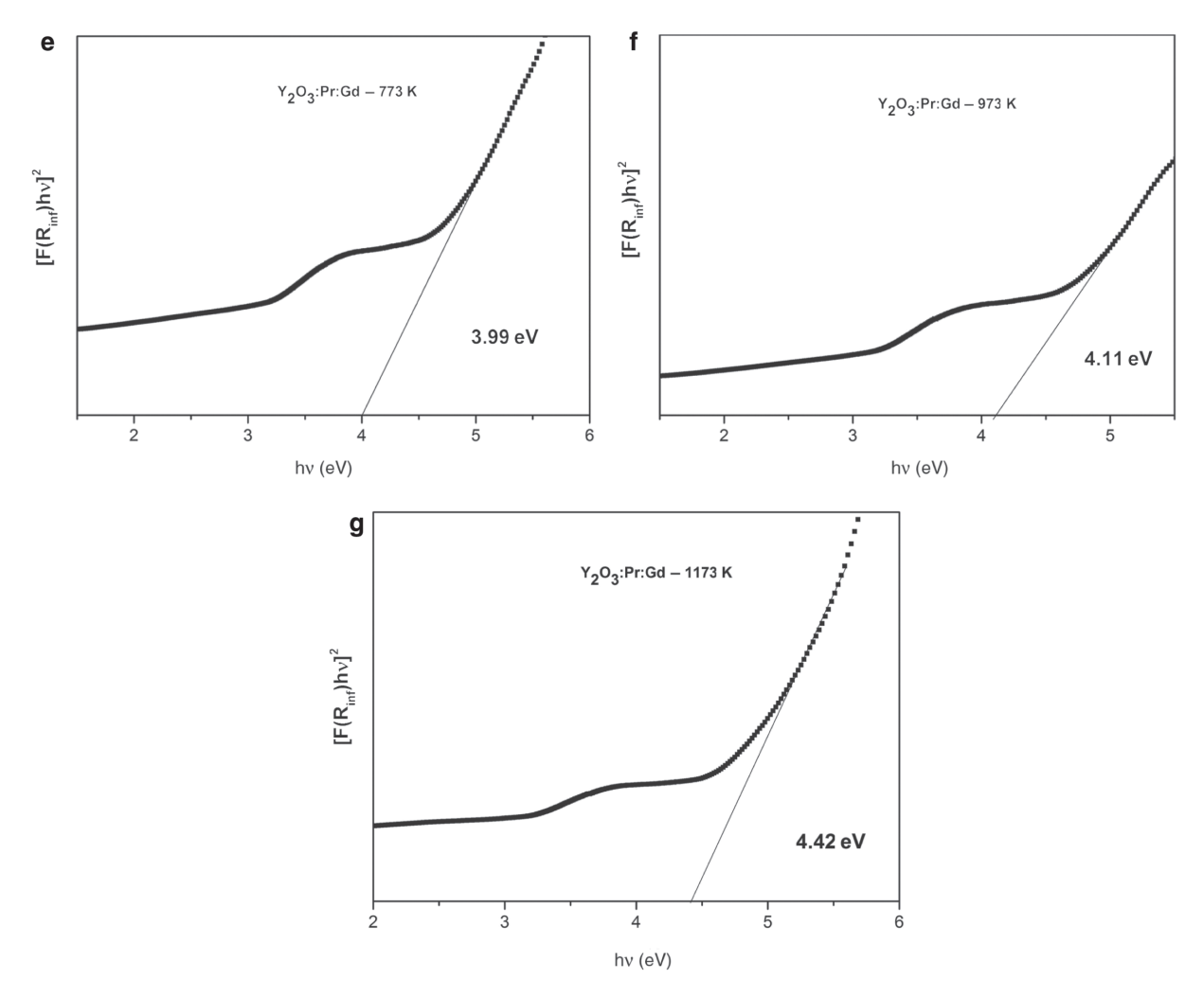


Figure 6: (continued)

Moreover, the distortion of lattice fringes is minimum [12]. It is clear that the reduction of particle size results in enhancement of surface area, which in turn increases the surface defects and ultimately results in the reduction of luminescence intensity [12]. Our sample exhibits good luminescence intensity. Because of this, more and more holes and electrons from the excited state will move to ground state through optically radiative recombination routes [12]. The particle size calculated from TEM is found to be in agreement with the size calculated from XRD studies [22].

The selected area electron diffraction (SAED) pattern of the sample heated at 1173 K is shown in Figure 7c and f. Studies reveal that the size and morphology of the Pr^{3+} -doped Y_2O_3 nanophosphor depend on some distinct parameters such as reaction temperature and time [40]. In the case of samples annealed at 1173 K, each particle contains several nanocrystals. This is the phase

transformation process from amorphous to crystalline [41]. Increase in temperature results in increase of particle size, decrease of surface-to-volume ratio, and scattering of light and finally results in increase of efficiency [41]. But at lower temperature, intensity is low. Imperfect incorporation of dopants into host lattice may be the reason for low luminescence intensity [41]. From FE-TEM, it was clear that Pr³⁺-doped nanophosphors exhibit crystalline nature with spherical shape. The sizes of the Pr³⁺-doped Y₂O₃ nanophosphors vary from 5 to 20 nm [42]. When we compare the particle size from TEM image and XRD line width, size is larger in the former case. The reason is that the line width depends on coherent domains, but TEM does not possess such requirement, and it measures the actual size [43]. Sintering plays an important role in size increment. The reason is the presence of hydrogen bonds that occurs between hydroxyl group results in oxygen bridge bonds [44]. The TEM image reveals the presence of some small

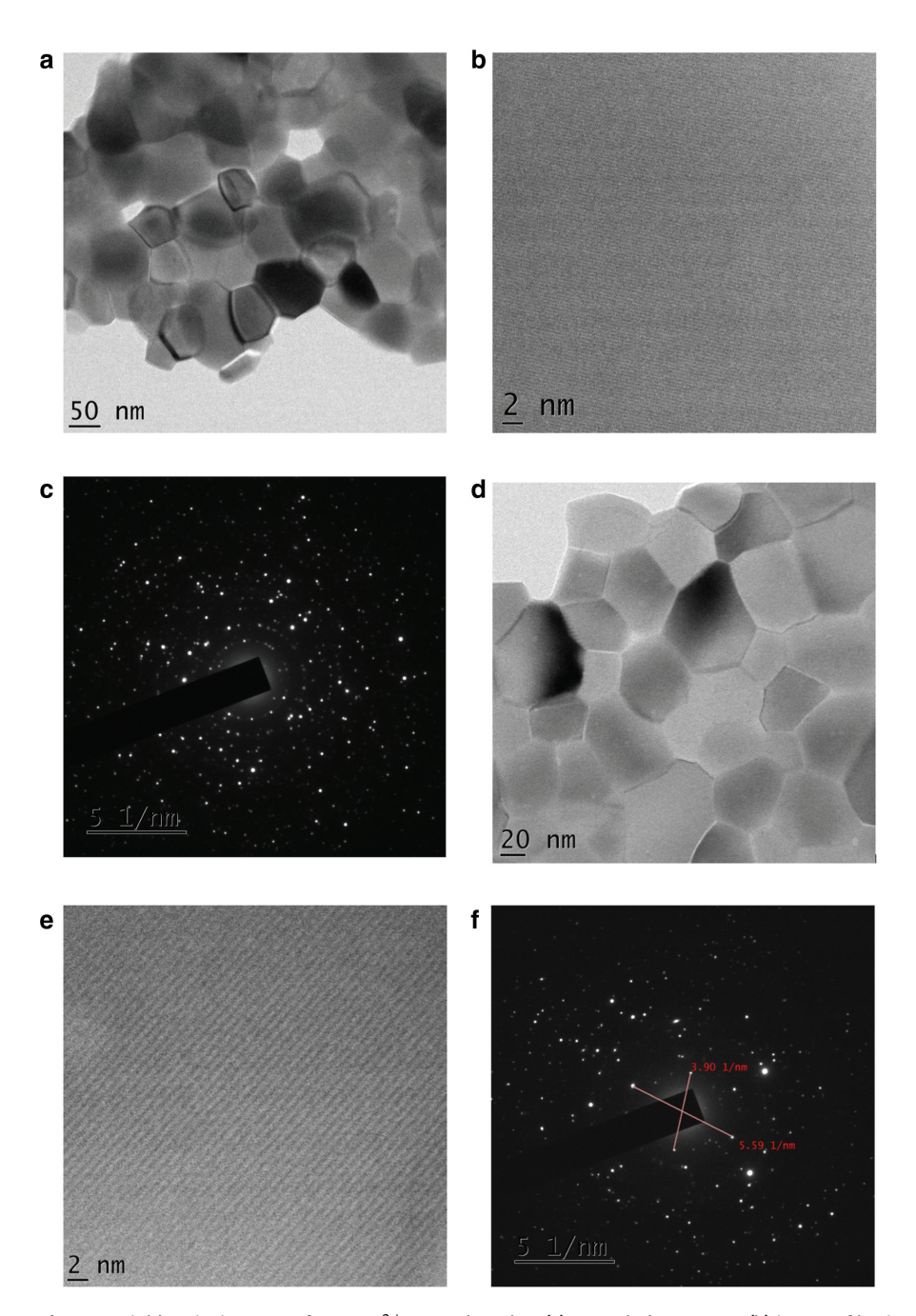


Figure 7: Field emission TEM of Y_2O_3 : Pr^{3+} nanophosphor (a) annealed at 1173 K; (b) image of lattice fringes and (c) SAED pattern. Field emission TEM of Y_2O_3 : Pr^{3+} : Gd^{3+} nanophosphor (d) annealed at 1173 K; (e) image of lattice fringes and (f) SAED pattern.

pores in the prepared samples, which might be due to evolution of gases during combustion. These porous samples are easy to grind to obtain finer powders [45].

3.2.3 Influence of pH on Photoluminescence

In this work, we mainly focussed on the effect of three parameters, namely, the effect of pH, concentration effect of Pr^{3+} ions, and effect of annealing temperature on the luminescence studies of Y_2O_3 nanophosphors. The

luminescence studies of Y_2O_3 doped with 2 wt% of Pr^{3+} , which was prepared in different pH values, are shown in Figure 8a. The PL emissions of all the samples exhibit strong and maximum peaks corresponding to a wavelength of 605 nm. The peak intensity increases with increase in pH up to a value of 8. When we further increase pH value, no intensity change can be observed. Same result can be obtained in the case of other samples, which was synthesised under various Pr^{3+} concentrations. Our studies thus indicate that a pH value of 8 gives much

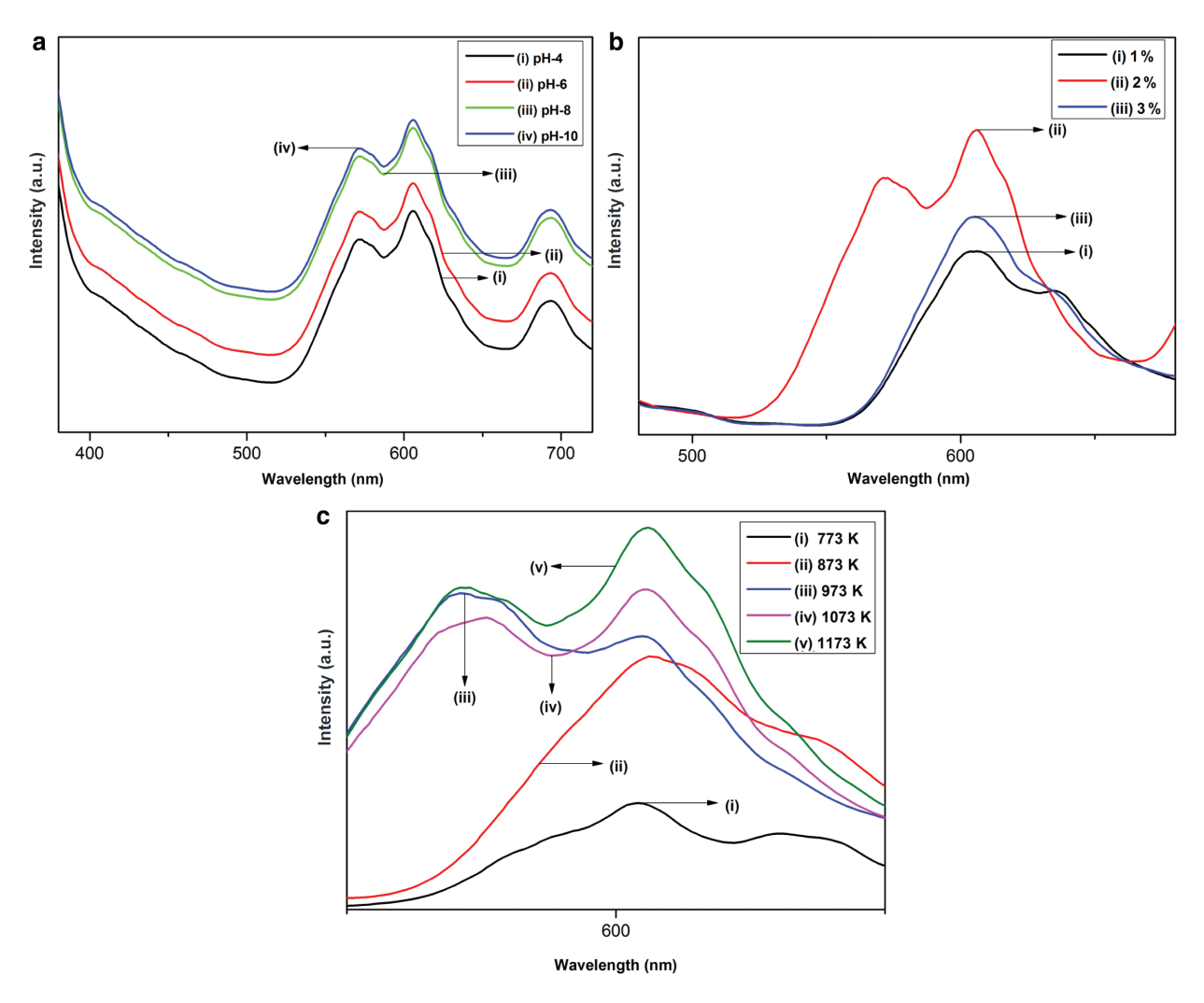


Figure 8: (a) PL emission spectra of 2 wt% Pr³⁺-doped Y₂O₃ prepared at different pH values. (b) PL emission spectra of 2 wt% Pr³⁺-doped Y_2O_3 prepared at different dopant values. (c) PL emission spectra of 2 wt% Pr^{3+} -doped Y_2O_3 annealed at different temperatures.

better luminescence intensity in the present prepared samples.

3.2.4 Influence of Doping Concentration on **Photoluminescence**

Luminescence studies have become one of the growing fields in material science because of industrial demands for new applications [46]. Luminescence phenomenon has been modified after the incorporation of Pr³⁺ ions into Y₂O₃ host lattice. This is because a large number of emission centres, which are capable to generate red colour, have been formed. It is understandable that the luminescence process that originates from 4f level transitions is mainly because of magnetic dipole or electric dipole transitions. The strongest emission peak around 605 nm is

due to electric dipole transition of ${}^{3}P_{0}$ to ${}^{3}H_{6}$, which is hypersensitive [46].

In order to verify the optimised dopant concentration. a series of Pr³⁺ concentrations of about 1 %-5 wt% were studied. The dependence of luminescence on the dopant concentration is shown in Figure 8b. When we change the concentration of Pr³⁺ dopant, the peak intensity changes, but there is no change in the peak position. As indicated in Figure 8b, initially, the luminescence intensity increases with increase in Pr³⁺ concentration. But then, the intensity of peak reduces when the concentration of Pr³⁺ exceeds the critical concentration value. In the case of Pr³⁺-doped Y₂O₃, the maximum peak intensity was observed when the concentration of dopant is 2 wt%. This trend of luminescence dependence on dopant concentration is found to be in accordance with earlier reported literature. Moreover, concentration of dopant is

not the only factor on which the luminescence depends. It also depends on other features such as nature of the host, size of particle, synthesis process, and temperature. This is because the luminescence phenomenon is connected to a cross section, exact position of energy level, dielectric constant, and phonon energy of the host material. There occur a large number of centres that exhibit luminescence in the emitting level. In this case, the luminescence intensity will be higher. When we increase the concentration of Pr³⁺ dopant, more ions that are excited are transited to a corresponding emitting level (for example, ³P₀ for Pr). Therefore, increasing the concentration of Pr³⁺ ions will increase the intensity of PL up to a critical concentration, of which the luminescence is maximum [40]. Further increase in dopant concentration results in a quenching process [35]. In our study, the quenching of luminescence occurs when the concentration exceeds 2 wt%. The reason for the luminescence quenching may be due to leaching out of Pr³⁺ when the dopant concentration is high in the reaction. For confirmation, we have done the calculation for cubic cell parameter in the case of all doped samples. From the result, we found lattice constant increases with increase in Pr³⁺ concentration. This increase can be assigned to the fact that the ionic radius of Pr³⁺ is slightly higher than Y³⁺ ions. This result suggests that there appears no leaching out of Pr³⁺ ions. Obviously, this unusual behaviour of luminescence can be due to some other reasons [35]. As the concentration quenching takes place in between the activators, the excessive incorporation of Pr³⁺ into Y₂O₃ results in the reduction of luminescence intensity [47]. The quenching process takes place only at a particular dopant concentration where the average distance between the centres that exhibit emission to support the transfer of energy reduces [48]. At very high Pr³⁺ concentrations, the interactions between the nearest neighbouring Pr³⁺ ions result in an output-limiting effect. The studies reveal that the quenching of luminescence can be due to transfer of energy between nearby luminescence centres through cross relaxation [40].

In detail, the distance between the impurity centres reduces with increase in Pr³⁺ concentration. In such cases, despite light emission, energy transfer takes place from one excited centre to another. The energy may lead to emission of light, but transfer enhances the probability of the occurrence of transition, which is nonradiative in nature [46]. Certain defects create localised levels, which are very deep with high ionisation energies. Electron–lattice interactions are usually strong in

these levels. Thus, the nonradiative recombination occurs through these levels [49]. Also, if the size and valence of the activator are not a match with the site in which they are substituted, it will be tedious to incorporate a huge amount of impurity. Thus, the optimal doping levels depend on the nature of both luminescent centre and host matrix [46]. The luminescence quenching due to concentration occurs when the emitting state loses the energy that is excited through cross-relaxation mechanism. This type of relaxation takes place between two similar nearby centres by transfer of energy resonantly. That means, in the case of two adjacent similar centres, transfer of energy occurs resonantly through cross relaxation. In that case, one centre that acts as donor transfers part of the energy that was excited to the nearby centre that acts as an acceptor [48]. The excitation migration increases with increase in concentration. Thus, the surfaces behave as centres for quenching or the energy attains remote killers [49]. This results in transfer of energy to defects that relax to their ground state by infrared or multiphonon emission [48]. Earlier studies reported that when the concentration of dopant is high, there may occur aggregation or pairing of dopant ions in which a small amount of activators act as killers [35, 43].

The luminescence quenching process in our study can be assigned to one or both mechanisms. The excitation energy migrates nonradiatively from one Pr³⁺ ion to its nearby Pr³⁺ ion by exchange interaction, which involves several transfer steps and ultimately to quenching site. When the Pr^{3+} dopant concentration is less than 2 wt%, the adjacent Pr³⁺ ions are found to be isolated. Only very few Pr³⁺ ions that have defects will transfer their energy to the nearby traps. Thus, the quenching process does not play an important role. When the concentration of the dopant increases to 2 wt%, the adjacent Pr³⁺ ions become closer enough to transfer energy that are excited, resonantly. When the concentration of dopant exceeds 2 wt%, the nearby Pr³⁺ becomes much closer to lose the energy nonradiatively that supports quenching process and reduction in luminescent intensity.

In the luminescence phenomena, the excited photons must possess energy that is less than the bandgap of the host. Thus, electrohole pairs are not produced. The excitation of luminescent centre is done by making use of a wavelength that lies in the absorption band that relaxes nonradiatively to the 3P_0 level. Then it radiatively relaxes to the ground state by emitting photons corresponding to specific transitions localized within the Pr^{3+} itself [48].

3.2.5 Influence of Annealing Temperature on Photoluminescence

The luminescence spectra of Pr^{3+} -doped Y_2O_3 nanophosphors annealed at various temperatures from 773 to 1173 K

are shown in Figure 8c. Here, we have taken the optimum concentration of dopant (2 wt%). This study reveals the dependence of luminescence on annealing temperature. From the graph, it is clear that the as-prepared samples exhibit weak luminescence intensity. Further, this

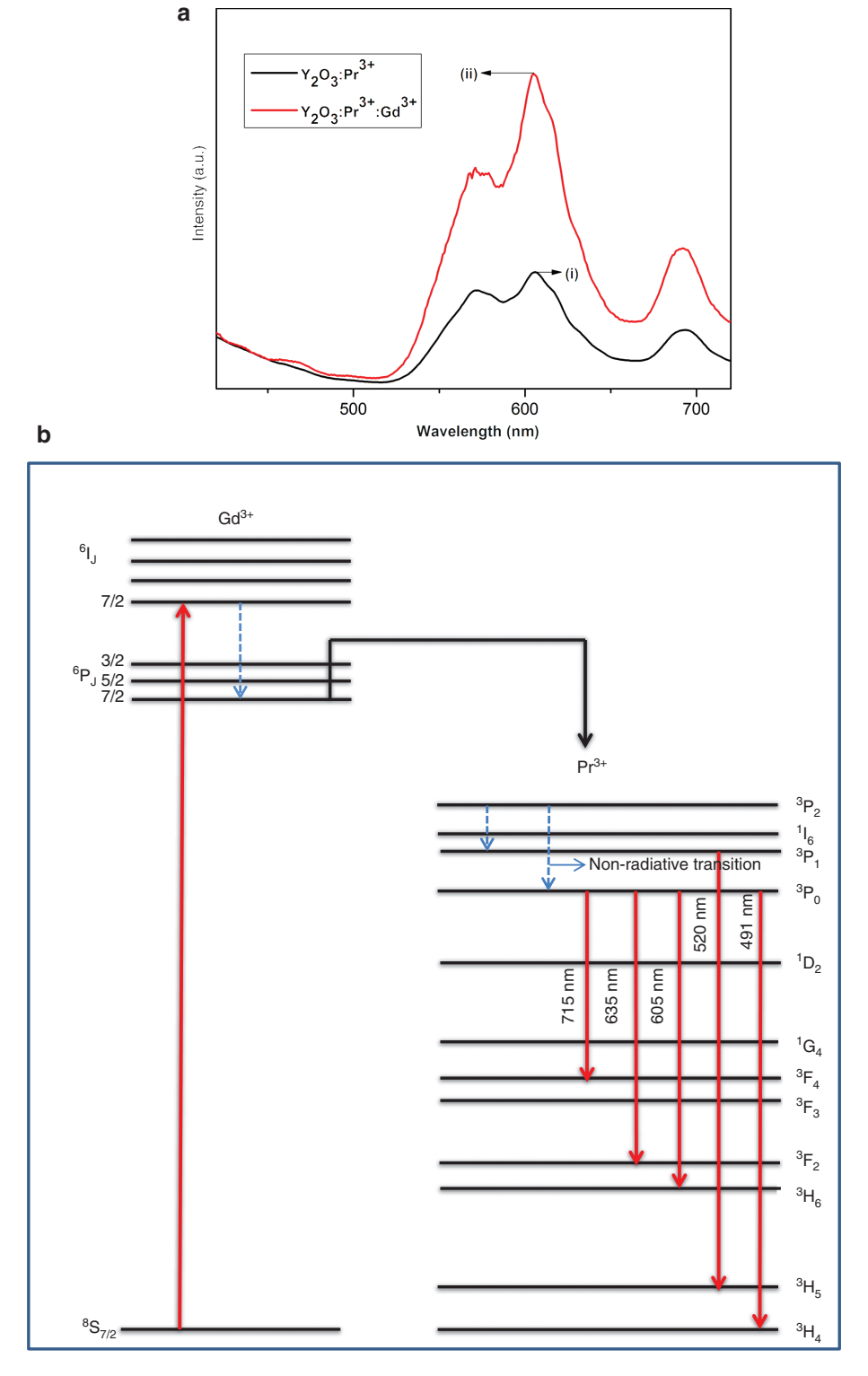


Figure 9: (a) Comparison of PL spectra of doped and co-doped samples. (b) Energy transfer diagram.

intensity increases with increase in temperature [37]. The increased intensity indicates good crystallinity. It also indicates that the dopant materials are properly incorporated into host matrix. These results are in good agreement with the XRD results [15]. This is because the synthesis of samples at high temperature supplies high energy. This results in good crystallite size and crystallinity. Enhancement of red emission can be done by increasing the oxygen vacancies, as reported by T. Yan et al. These oxygen vacancies normally act as radiative centres in luminescence process [50]. The as-prepared samples exhibit low PL yield, which may be due to high surface-tovolume ratio of nanophosphors. The size increment with temperature results in the decrease of surface-to-volume ratio, which in turn enhances the luminescence intensity. The peak intensity and peak position give information regarding the nature of Pr^{3+} environment in Y_2O_3 nanophosphors. ³P₀ to ³H₆ transition is responsible for the red emission at 605 nm [37]. Other transitions of Pr³⁺ are also visible but found to be very weak. Moreover, our sample does not exhibit the presence of monoclinic phase. If the sample exhibits monoclinic phase, the maximum emission ³P₀ to ³H₆ will be at a wavelength of 623 nm. Thus, we confirmed that the combustion method results in the formation of single-phase cubic Pr-doped vttrium nanophosphors [43]. Peak intensity increases with increase in temperature as we discussed earlier. When we make a comparison between the samples in as-prepared condition and annealed at 973 K, quite interestingly, we obtained nearly 2.58 orders of intensity increment in the case of annealed samples. Attainment of good crystallinity may be the reason for this as indicated in XRD studies. Many authors reported the dependence of luminescence on particle size. In our case, we observed that the particle size increase with increasing temperature. X-ray diffraction studies also revealed the enhancement of crystallinity with temperature. Thus, we can confirm that increment of peak intensity with increase in temperature can be assigned to enhanced crystallinity of yttrium nanophosphors [35]. Even though the particle size varies with temperature, the peak position remains unchanged [16].

There is a direct dependence of luminescence on morphology of \Pr^{3+} -doped Y_2O_3 nanophosphors. It is clear that when we compare nanospheres and nanorods, intensity emission is more for nanospheres. This confirms that spherical-shaped samples exhibit good luminescence phenomena. This is because this particular spherical shape reduces the light-scattering effect and nonradiation. The \Pr^{3+} -doped Y_2O_3 nanophosphors that we obtained have spherical shape without agglomeration. This can be

applied in various fields such as field emitters, laser materials, and optoelectronic devices [50].

3.2.6 Influence of Co-doping on Photoluminescence

The incorporation of gadolinium oxide into the Pr³⁺doped Y2O3 nanophosphors results in the enhancement of luminescence. By keeping the value of Pr³⁺ as constant (2 wt%), we added different concentrations of Gd³⁺ and finally obtained 1 wt% of Gd³⁺ as the optimised codoped value. Figure 9a shows the comparison graph of doped and co-doped samples. Gd³⁺ incorporation does not make any change in the position of the peak that corresponds to ³P₀ to ³H₆ transition, but it enhances the intensity peak, which indicates that Gd³⁺ sensitises the red emission perfectly through transferring the energy from Gd³⁺ to Pr³⁺ [29]. Intensity of 605-nm emission increases with Gd³⁺ addition linearly. The intensity of Y:Gd:Pr sample is 2.705 times that of the Y₂O₃:Pr sample. Addition of Gd³⁺ results in covalency increment. By considering the bond structure of Pr^{3+} - O^{2-} - Y^{3+} / Gd^{3+} , we found that electronegativity values of Y^{3+} and Gd^{3+} are 1.22 and 1.20, respectively. The electron-ion attraction takes place in the form $Y^{3+} > Gd^{3+}$. Thus, in the same way, the energy that is required for electron transfer from 0^{2-} to Pr³⁺ increases. The replacement of Y³⁺ with Gd³⁺ makes transfer of charge easier, which in turn leads to luminescence enhancement. Energy transfer diagram is given in Figure 9b.

4 Conclusions

The XRD studies confirm that the incorporation of Pr³⁺ and Gd³⁺ ions does not make any change in the structure of the Y₂O₃. It has been found that when the annealing temperature increases, the particle size and crystallinity of the nanophosphors increase. The FTIR studies indicate that the presence of hydroxyl group (OHOH) and CO₂ group in as-prepared samples vanishes when the temperature increases, which in turn results in the enhancement of luminescence properties. Eg values have been calculated from DRSs. For doped samples, Eg values vary from 4.63 to 5.00 eV, and for co-doped samples, it varies from 3.99 to 4.42 eV. This bandgap difference can be because of size difference. Analysis of PL emission has been done, and the emission peak was at 605 nm, which was due to ${}^{3}P_{0}$ -to- ${}^{3}H_{6}$ transition. The results show that when the concentration of dopant increases the luminescence intensity also increases up to optimised value. Moreover, the optimum concentration was obtained at 2 wt% Pr³⁺. The luminescence intensity has been enhanced after the addition of Gd³⁺ as co-dopant. The [Y:Pr:Gd] exhibits luminescence intensity of 2.705 times more than that of Y:Pr nanophosphors.

References

- [1] A. Towata, M. Sivakumar, K. Yasui, T. Tuziuti, T. Kozuka, et al., J. Mater. Sci. 43, 1214 (2008).
- [2] T.-Y. Hwang, Y. Choi, Y. Song, N. S. A. Eom, S. Kim, et al., J. Mater. Chem. C 6, 972 (2018).
- [3] X. Huang, Nat. Photonics 8, 748 (2014).
- [4] X. Huang, Sci. Bull. 64, 879 (2019).
- [5] J. Liang, P. Du, H. Guo, L. Sun, B. Li, et al., Dyes Pigments 157, 40 (2018).
- [6] X. Huang, S. Wang, B. Li, Q. Sun, and H. Guo, Opt. Lett. 43, 1307 (2018).
- [7] X. Li, Z. Yang, L. Guan, Q. Guo, C. Liu, et al., J. Alloys Compd. 464, 565 (2008).
- [8] N. Vu, T. Kim Anh, G.-C. Yi, and W. Strek, J. Lumin. 122, 776 (2007).
- [9] S. Zhou, Z. Fu, J. Zhang, and S. Zhang, J. Lumin. 118, 179 (2006).
- [10] N. Mohamed, J. Hassan, K. A. Matori, R. S. Azis, Z. A. Wahab, et al., Results Phys. 7, 1202 (2017).
- [11] M. Okumura, M. Tamatani, A. K. Albessard, and N. Matsuda, Jpn. J. Appl. Phys. 36, 6411 (1997).
- [12] B. K. Gupta, D. Haranath, S. Saini, V. N. Singh, and V. Shanker, Nanotechnology 21, 055607 (2010).
- [13] J. Hao, S. A. Studenikin, and M. Cocivera, J. Lumin. 93, 313 (2001).
- [14] K. M. Nissamudeen and K. G. Gopchandran, J. Optoelectron. Adv. M. 10, 2719 (2008).
- [15] S. Som, S. K. Sharma, and T. Shripathi, J. Fluoresc. 23, 439 (2013).
- [16] L. Robindro Singh, R. S. Ningthoujam, V. Sudarsan, I. Srivastava, S. Dorendrajit Singh, et al., Nanotechnology 19, 055201
- [17] R. Srinivasan, R. Yogamalar, A. Vinu, K. Ariga, and A. C. Bose, J. Nanosci. Nanotechnol. 9, 6747 (2009).
- [18] J. R. Jayaramaiah, K. R. Nagabhushana, and B. N. Lakshminarasappa, J. Anal. Appl. Pyrolysis 123, 229 (2017).
- [19] S. P. Peddi, H. Mathlouthi, B. A. Sadeh, and Y. M. Abdelhaye, AUSEJ 4, 1 (2017).
- [20] K. M. Nissamudeen, R. G. A. Kumar, V. Ganesan, and K. G. Gopchandran, J. Alloys Compd. 484, 377 (2009).
- [21] T. Sh. Atabaev, H. H. Thi Vu, H.-K. Kim, and Y.-H. Hwang, J. Alloys Compd. 525, 8 (2012).
- [22] P. Packiyaraj and P. Thangadurai, J. Lumin. 145, 997 (2014).

- [23] D. Y. Medina Velazquez, L. A. Hernández Soto, Á. de J. Morales Ramirez, S. Carmona-Téllez, E. Garfias-Garcia, et al., Ceram. Int. 41, 8481 (2015).
- [24] A. Boukerika and L. Guerbous, J. Lumin. 145, 148 (2014).
- [25] F. Voicu, C. Gheorghe, and C. Florica, Ann. West Univ. Timisoara Phys. 56, 76 (2012).
- [26] R. Priya and O. P. Pandey, J. Lumin. 212, 342 (2019).
- [27] J. Li, Y. Wang, and B. Liu, J. Lumin. 130, 981 (2010).
- [28] T. Verma and S. Agrawal, J. Mater. Sci. Mater. El. 29, 13397 (2018).
- [29] J.-G. Li, X. Li, X. Sun, and T. Ishigaki, J. Phys. Chem. C 112, 11707 (2008).
- [30] J. R. Jayaramaiah, B. N. Lakshminarasappa, and K. R. Nagabhushana, J. Lumin. 157, 63 (2015).
- [31] V. Dubey, S. Agrawal, and J. Kaur, Indian J. Mater. Sci. 2014, 1 (2014).
- [32] S. Ćulubrk, V. Lojpur, Ž. Antić, and M. D. Dramićanin, J. Res. Phys. 37, 39 (2013).
- [33] C. A. Kodaira, R. Stefani, A. S. Maia, M. C. F. C. Felinto, and H. F. Brito, J. Lumin. 127, 616 (2007).
- [34] M. K. Devaraju, S. Yin, and T. Sato, J. Nanosci. Nanotechnol. **10**, 731 (2010).
- [35] G. Siddaramana Gowd, M. K. Patra, S. Songara, A. Shukla, M. Mathew, et al., J. Lumin. 132, 2023 (2012).
- [36] J. Zhang, Z. Zhang, Z. Tang, Y. Lin, and Z. Zheng, J. Mater. Process. Technol. 121, 265 (2002).
- [37] R. Hari Krishna, B. M. Nagabhushana, H. Nagabhushana, N. Suriya Murthy, S. C. Sharma, et al., J. Phys. Chem. C 117, 1915 (2013).
- [38] R. Priya and O. P. Pandey, Vacuum 156, 283 (2018).
- [39] R. A. Mir, P. Sharma, and O. P. Pandey, Sci. Rep. 7, 3518 (2017).
- [40] H. Huang, H. Zhang, W. Zhang, S. Lian, Z. Kang, et al., J. Lumin. 132, 2155 (2012).
- [41] Y. D. Jiang, Z. L. Wang, F. Zhang, H. G. Paris, and C. J. Summers, J. Mater. Res. 13, 2950 (1998).
- [42] X. Jing, J. Electrochem. Soc. 146, 4654 (1999).
- [43] A. Gupta, N. Brahme, and D. Prasad Bisen, J. Lumin. 155, 112 (2014).
- [44] C. He, Y. Guan, L. Yao, W. Cai, X. Li, et al., Mater. Res. Bull. 38, 973 (2003).
- [45] Y.-P. Fu, J. Mater. Sci. 42, 5165 (2007).
- [46] M. Nazarov and D. Noh, New Generation of Europiumand Terbium-Activated Phosphors: From Syntheses to Applications, Pan Stanford Pub, USA 2011.
- [47] G. Y. Hong, B. S. Jeon, Y. K. Yoo, and J. S. Yoo, J. Electrochem. Soc. 148, H161 (2001).
- [48] G. H. Mhlongo, M. S. Dhlamini, H. C. Swart, O. M. Ntwaeaborwa, and K. T. Hillie, Opt. Mater. 33, 1495 (2011).
- [49] W. M. Yen, S. Shionoya, and H. Yamamoto, Practical Applications of Phosphors, Taylor and Francis Group, Abington, Oxford, United Kingdom 2007.
- [50] T. Yan, D. Zhang, L. Shi, H. Yang, H. Mai, et al., Mater. Chem. Phys. 117, 234 (2009).